Plasma-catalysis coupling for CH4 and CO2 conversion over mesoporous macroporous Al2O3: Influence of the physico-chemical properties

Nassim Bouchoul, Houcine Touati, Elodie Fourré, Jean-Marc Clacens, Isabelle Batonneau-Gener, Catherine Batiot-Dupeyrat

Plasma-catalysis coupling for CH_4 and CO_2 conversion over mesoporous macroporous Al_2O_3: influence of the physico-chemical properties

Nassim Bouchoul, Houcine Touati, Elodie Fourré, Jean-Marc Clacens, Isabelle Batonneau-Gener, Catherine Batiot-Dupeyrat*

IC2MP, ENSIP, Université de Poitiers - UMR CNRS 7285
1 rue Marcel Doré, TSA 41105, 86073 Poitiers cedex 9 (France)

*E-mail : catherine.batiot.dupeyrat@univ-poitiers.fr

Abstract

Macro-mesoporous alumina, calcined at different temperatures (from 400 to 800 °C), were tested in dry reforming of methane reaction under plasma discharge at a fixed deposited power (P = 8 W) with a ratio CO_2/CH_4 = 2. Besides alumina materials, the one possessing the lowest surface area (72 $m^2\ g^{-1}$) exhibited the highest activity: Methane conversion reaches 31.3 % against 23.4, 22.6 and 26.8 % for alumina calcined at 400, 600 and 800 °C, respectively, suggesting that the active sites generated into the mesoporosity of alumina (Al_2O_3 400) are not accessible to reactants under the plasma discharge. Reactant transformation is promoted with the alumina possessing the highest number of acid and basic sites and a correlation is proposed. It is believed that CH_4 and CO_2 adsorption are improved over acid and basic sites at the surface of alumina, favoring the production of syngas.

1. Introduction

For many years, plasma catalysis has been developed in different application fields such as air pollution control [1], ammonia synthesis [2], reforming reactions [3], CO_2 hydrogenation [4, 5], catalyst regeneration [6], as listed in "the 2020 plasma catalysis roadmap" [7].

The combination of plasma with a catalyst for the reaction of dry reforming of methane (DRM) has been investigated to overcome the main drawbacks of the two separated techniques: catalyst deactivation by coke deposition at high temperature due to the high endothermicity of the reaction and a poor selectivity achieved with non-thermal plasmas [8-12]. In the hybrid system, catalysts similar to those used in conventional thermal catalytic processes, such as Ni/SiO_2, Ni/Al_2O_3 or Pt/Al_2O_3, Pd/Al_2O_3 [13-15], were inserted in the plasma discharge region. In some studies, the presence of reduced Ni species in the discharge showed a small positive effect in comparison with plasma only [16, 17], while other authors obtained a decrease in conversions of CH_4 and CO_2 [18].

It is unanimously accepted that the presence of a solid in the plasma region modifies significantly the discharge, particularly if the material is conductive [3]. Jo et al. [19] proposed that the electric field is weakened by the electric conductivity of the solid, reducing the electron density and thereby lowering the reactants conversion. Moreover, Kim et al. [20] demonstrated that the bulk temperature strongly influences the C-H bond activation of methane, CH_4 conversion increasing more than 8 fold in the presence of Ni/Al_2O_3 but only at temperature higher than 630 K.

In the different published papers, the authors used a specific catalyst composition and comment on the beneficial effect of the coupling leading to synergetic effect (in some cases). In a review, Chung [21] listed different catalysts used to perform the DRM reaction coupled with plasma and the authors concluded that plasma and catalyst interactions depend on many parameters

such as operating temperature, basicity of the catalyst, power input, dielectric constant, reactor geometry and catalyst packing method.

Using a zeolite A, Jiang et al. [22] showed that CH_4 and CO_2 conversions were reduced, but the formation of carbon black was inhibited. Metal-organic-frameworks (MOFs) was successfully used by Vakili et al. [23] in the plasma-assisted dry reforming of methane, the improved CH_4 and CO_2 conversion compared to the plasma-alone mode was attributed to the favorable generation of filamentary micro discharges and surface discharges with the highly porous material.

An important point is that the combination of plasma with simple oxides possessing no thermal activity exhibited higher performances compared with plasma only: a significant improvement in CH_4 and CO_2 conversion over Al_2O_3 and La_2O_3/Al_2O_3 was observed when coupled with plasma at 573 K [24]. A higher CO_2 conversion and a lower CH_4 conversion were reported by Zhang et al. [25] using La_2O_3/Al_2O_3 under pulse corona plasma. Michielsen et al. [26] have shown that α-Al_2O_3 and γ- Al_2O_3 are beneficial for CO_2 and CH_4 conversion compared to other oxides such as ZrO_2, SiO_2, or $BaTiO_3$. In a recent paper [27] we studied the dry reforming of methane by non-thermal plasma coupled with different metal oxides: BaO, La_2O_3, ZnO, CaO, α-Al_2O_3, MgO, γ-Al_2O_3, TiO_2 and CeO_2 and it was observed that the CO_2 and CH_4 conversions were enhanced when the permittivity of solid was reduced, the best results being obtained with γ-Al_2O_3.

In this context the main objective of the present study was to investigate the influence of physico-chemical properties of different alumina oxides compared to a commercial gamma alumina. The aim was to correlate the physico-chemical properties of the solid to the CH_4 and CO_2 transformations in a single plasma reactor at a fixed deposited power.

2. Experimental part

2.1 Experimental setup

The reaction was performed in a coaxial dielectric barrier discharges (DBD) reactor (Fig. 1) at room temperature and atmospheric pressure. The reactor is an alumina tube with 4mm internal and 6 mm external diameter. A stainless steel rod (diameter: 1mm) is centered inside the alumina tube and set as the high voltage electrode while a copper electrode (100 mm long) is wrapped around it and set as the ground electrode.

Helium, CH_4 and CO_2 were flown at a total flow rate of 40 mL min^{-1} (residence time of 1.6 s) with a ratio CO_2/CH_4 of 2 and a constant concentration in He (75 %).

The material (alumina) filled the entire plasma zone. Powders were sieved before experiments in the range: 355-650 µm, since we showed in a previous study that it corresponds to an optimized grain size to perform the reaction under plasma discharge [28]. The advantage of using small grains has also been highlighted by Kasinathan et al. for the CH_4 conversion into hydrocarbons over MgO/Al_2O_3 [29] and by Zhou et al. [30] for the decomposition of CO_2 on ZrO_2.

A sinusoidal AC supply of power was applied across the electrode (TG1010A Aim-TTi, Thurlby Thandar Instruments Brand). The discharge power was calculated through the figure of Lissajous and fixed at 8 watts, while the frequency was kept constant at 800 Hz. The voltage was varied from 13.2 to 14.3 kV depending on the nature of the material in order to fix the deposited power at 8W. The applied voltage was measured with high voltage probes (PMK, model PHV4-2757) using an oscilloscope (waveRunner 62 Xi, Lecroy).

An Ametek ®, Solartron Analytical apparatus was used to determine dielectric constants of oxides: a sinusoidal voltage of 50 V was applied with a scan from 0,1 Hz to 1 MHz. The oxides were pressed at 5 tons for measurements, producing wafers of 2 mm thick that allows to neglect

the contribution of air permittivity. Before analysis, wafers were placed in an oven at 100 °C to avoid water adsorption.

2.2 Al_2O_3 synthesis and characterization

Mesoporous macroporous alumina were prepared according to the procedure inspired by Z-Y. Yuan et al. [31]: 10.42 g of cetyltrimethylammonium bromide (CTMABr) were dissolved in 93.93 g of deionized water. The suspension was stirred at 40 °C for 1 h before the addition of 24.12 g of aluminum isopropoxide, under stirring. The resulting gel was further agitated for 3 h at 40 °C. The obtained gel was placed in a closed polypropylene bottle at 80 °C for 24 h, under static conditions. After a cooling down at room temperature, the suspension was filtered and washed with water (200 ml, 2 times). The resulting paste was dried at 100 °C overnight. The obtained powder was washed again with 200 ml of water, and then dried overnight at 100 °C. Finally, the obtained alumina was calcined at 400, 600 or 800 °C for 6 h (heating rate: 2 °C min^{-1}). Characterization of the materials was carried out before and after reaction under plasma. The specific surface areas were obtained according to the BET procedure. The nitrogen adsorption-desorption isotherms were carried out using a Micromeritics Flowsorb II 2300 apparatus at -77 K. The commercial γ-alumina was purchased from Alfa Aesar (CAS: 1344-28-1). It was calcined before use at 400 °C for 6h (heating rate: 2 °C min^{-1}) and noted γ-Al_2O_3.

The surface acidity was measured by temperature programmed desorption of ammonia (NH_3-TPD). NH_3-TPD experiments were carried out using a homemade apparatus equipped with a TCD detector. Prior to the measurements, about 80 mg of sample were pretreated by heating at 200 °C for 1 h under helium with a ramp of 5 °C min^{-1}, and, after cooling for 5 min to 30 °C, ammonia adsorption was carried out. A flow of 30 mL min^{-1} containing 5 vol % NH_3 in helium was passed over the sample during 45 minutes at 30 °C. Physically adsorbed ammonia was removed by purging with helium at 50 °C for 3 h. The NH_3-TPD was carried out by increasing

the temperature linearly from 50 to 600 °C with a heating rate of 5 °C min^{-1} and a helium flow rate of 30 mL min^{-1}.

The amount of acidic sites on the catalyst was calculated from the desorption amount of NH_3, which was determined by measuring the areas of the desorption profiles.

In a previous work, we have shown that the amount of CO_2 adsorbed in the monolayer is directly linked to the basic site number present at the material surface [32]. CO_2 monolayer content was calculated from the analysis of CO_2 adsorption isotherm by BET model. Adsorption equilibrium data were measured at 25 °C using a symmetrical SETARAM microbalance. 40 mg of samples were out-gassed under secondary vacuum at 350 °C for 12 h and cooled down to 25 °C prior to the sorption measurements. The temperature of the system was kept constant during analysis by a water circulation in the double walls of the analysis tubes. The CO_2 pressure was then increased step by step in order to obtain the entire adsorption isotherm. For each uptake, the equilibrium was reached when the mass recorded versus time and the pressure were stable.

Thermogravimetric analysis were performed with a TA instruments SDTQ600 analyzer under a 50 mL min^{-1} flow of air to 900 °C (10 °C min^{-1}).

Thermogravimetric analysis coupled with mass spectrometry (TGA-MS) were performed on a SDT Q600 apparatus from TA Instruments coupled by a heated capillary column with a QGA mass spectrometer from Hiden. The samples were heated up to 800 °C (heating rate: 10 °C min^{-1}) under an air flow (50 mL min^{-1}).

The catalysts were characterized by X-Ray Diffraction (XRD) using a Siemens D-5005 diffractometer with CuKα = 1.5417 Å, operated at 40 kV and 30 mA. The diffraction patterns were recorded in the 2θ range of 10-90 ° with a step interval of 0.02 ° and period of 1 s.

2.3 Gas phase analysis and calculation

The gas analyses were conducted on-line by gas chromatography. A flame ionization detector allowed the identification of oxygenated products, while a thermal conductivity detector

identified the hydrogen, carbon monoxide, carbon dioxide and methane. All the reactions lasted 1 hour.

Each experiment was repeated 3 times, changing the catalyst and cleaning the inner electrode each time, resulting in a margin error of ± 3 %.

The conversion, yield, selectivity and energy efficiency were defined as:

Conversion (%) of CH_4 and CO_2 = 100 × mole of CH_4 (or CO_2) converted / mole of CH_4 (or CO_2) in the feed

Yield in H_2 (%) = 100 × mole of H_2 / 2 x (mole of CH_4) introduced

Selectivity to C_nH_y (%) = 100 × n × mole of C_nH_y / (mole of CH_4 converted + mole of CO_2 converted)

Selectivity to CO (%) = 100 × mole of CO / (mole of CH_4 + mole of CO_2) converted

Carbon Balance: CB (%) = 100 × (mole of CO +$\sum$ n × mole of C_nH_y) / (mole of CH_4 converted + mole of CO_2 converted)

3 Results and discussion

3.1 Textural properties of alumina

The BET specific surface area, BJH desorption cumulative pores volume and average pore width are gathered in Table 1. As expected, the alumina materials synthesized in the laboratory possess a large surface area compared to the commercial alumina. As the calcination temperature increases from 400 to 800 °C, the S_{BET} decreases from 313 to 261 $m^2 g^{-1}$. The pore volumes are low especially for the gamma alumina with the lowest surface area. Nitrogen adsorption desorption isotherms and pore size distributions are shown in Fig. 2. According to the IUPAC classification, the prepared alumina exhibit type IV isotherm with H2 hysteresis loop, typical of mesoporous materials with a complex porosity. The commercial γ-Al_2O_3 exhibits a loop of type IIb, indicating the presence of macropores, the porosity being not

completely filled by N_2 condensation [33]. The pore size distribution (Fig. 2) confirms the presence of large pores for the commercial alumina (dV/dD pore volume maximum around 400 Å – average pore diameter of 142 Å), while for the materials synthesized in the laboratory, this maximum is around 50 Å (average pore diameter from 42 to 72 Å).

The SEM images (Fig. 3) show the presence of abundant pores whatever the calcination temperature 400, 600 or 800°C.

XRD patterns of γ-Al_2O_3, Al_2O_3 400, Al_2O_3 600 and Al_2O_3 800 are presented in Fig. 4. They all show the representative diffraction peaks of gamma alumina (ICDD 00-010-0425).

3.2 Physical and electrical discharge characteristics of alumina packed plasma reactor

Substantial alterations are observed for the Lissajous Q-V curves of the four alumina oxides (Fig. 5). Note that a peak voltage of 13.2kV was required to obtain a deposited power of 8W for Al_2O_3 600, while 14.3 kV was used for γ-Al_2O_3. The charges accumulated at the surface of the dielectric material and the capacitances slightly differ between materials. Lines BC and DA correspond to the plasma-off phase, the slope of these lines gives C_{cell} (capacitance of the dielectric and of the gap). The discharge-on is represented by lines AB and CD, the slope of these lines corresponding to the effective capacitance (Table 2). The differences in capacitances prove that the electrical properties of the alumina oxides are different, whereas similar grain size was used (355-650 µm). Note that the lowest values were obtained for the commercial alumina material, which also has the smallest surface area. The effective capacitance is supposed to depend on the spatial distribution of the discharge across the discharge gap. The higher value obtained for the prepared γ-Al_2O_3 can be explained by the expansion of the discharge at the surface of the alumina material [34].

The dielectric constant measurements of the alumina materials were low (2-4) compared to those reported in the literature for α- and γ-alumina (generally between 9 and 10) [35-37]. These

differences can be explained from the different measurement methodology followed. In this work, dielectric constants were measured experimentally, while published data were determined mathematically, as a sum of electronic and lattice contributions in most cases. The differences could come from the interfacial polarizations originating from sub-grain boundary and grain boundary barriers [38], which is not taken into account when the data come from calculation.

3.3 Influence of the type of alumina for CH_4 and CO_2 conversion

The alumina materials, freshly calcined at 400 °C and sieved in the range 355-650 µm, were introduced into the reactor, filling completely the plasma zone. The deposited power was adjusted at 8 W (13.2-14.3 kV and 800 Hz). The conversion of methane and carbon dioxide are plotted versus the surface area in Fig. 6. The highest conversions were obtained with the commercial alumina, possessing the lowest surface area: 72 m^2 g^{-1}, methane conversion reached 31.3 % against 23.4, 22.6 and 26.8 % for alumina calcined at 400, 600 and 800 °C, respectively. From these results, it seems that the active sites localized into the mesoporosity of alumina (Al_2O_3 400, 600 and 800) are not accessible to reactants under the plasma discharge. The accessibility of the porosity of solid is a key point in DBD plasma conditions. In fact, the formation of micro-discharges is possible only when the pores diameter is larger than the Debye length value, which lies between 100 nm to 1µm. This value depends on the electron density and temperature of the plasma streamer. A. Bogaerts group showed that plasma can diffuse in pores of about 50 nm, corresponding to the upper limit size of mesopores, but to a certain extent and in a very limited time period [39, 40]. Nevertheless, in a study on VOC removal by non-thermal plasma using a γ-Al_2O_3, Roland et al. [41] suggested the stabilization of short-lived oxidant species on the surface and their diffusion from gas phase into the pores of 7.4 nm (diameter). Moreover, based on EPR spectroscopy, the authors [42] proposed the formation of

an Al-O-O$^{\bullet}$ aluminium peroxyl group via oxygen present in the gas atmosphere. The results obtained in the present study showed experimentally that the coupling of plasma with catalyst depends strongly on the nature of surface active species (presence of OH) and in a lower extend to the amount of active sites as soon as there are located in small pores of oxides. Results in Table 3 reveals that the hydrogen yield and selectivity towards C_2H_6 are maximum for the commercial γ-Al_2O_3 compared to the other Al_2O_3 materials. Oxygenates were formed only when using the commercial alumina, the main products being formaldehyde > acetone > methanol > acetaldehyde > ethanol. However, the amount of oxygenates remains very low. The experimental conditions (excess of CO_2), not favorable for oxygenates production, were chosen to avoid carbon deposition [43]. The formation of oxygenates was also reported by Li et al. [44] using SiO_2 coupled with plasma in an excess of CO_2, they obtained mainly methanol, ethanol and acetic acid. In our study, the carbon balance is always lower than 100% especially in the presence of alumina with the highest surface area, suggesting that other products, not analyzed by GC, are formed. They could be hydrocarbons other than C2, because insignificant amount of ethylene and acetylene were detected. The formation of volatile oxygenated products such as ethers, peroxides or carboxylic compounds could also be produced, along with carbon deposition and/or product condensation at the surface of the material or in the setup lines.

DRM was studied by different groups using Al_2O_3 as packing material (Table 5). Important differences in terms of reactant conversion and selectivity to products are observable. These differences could be explained by the reactor design (gap, volume of plasma discharge…) and process conditions. Note that comparison between non-packing and packing reactor makes no sense if the gas flow is not adjusted in order to maintain the contact time at the same value. This aspect is unfortunately rarely taken into account in many papers. Nevertheless from the reported data, it appears that high deposited power promotes the selectivity to CO [45-47]. Michielsen et al. [26] show that α-Al_2O_3 material exhibits a slightly higher activity than γ-Al_2O_3,

suggesting that other effects than surface area or dielectric constant explain the results. The authors propose that the surface acidity of the material may lie at the base of this observation. In order verify this hypothesis, the influence of the number of acid and basic sites per unit surface of the alumina materials on CH_4 and CO_2 conversion was verified (Fig. 7). The highest activity is obtained with the commercial alumina exhibiting the highest number of acid and basic sites. Note that the acidity of γ- Al_2O_3 is associated with the ionic nature of the Al-O bond [48]. More specifically the acid sites would be localized closed to the –OH groups of the surface [49]. The role of acid sites in methanol production was proposed by Chawdhury et al. [50]. The authors obtained higher selectivity to oxygenates using Cu/γAl_2O_3 catalyst presenting more acid sites than Fe/γAl_2O_3 in the plasma-catalytic partial oxidation of methane. Also, the presence of basic sites favors the reactant conversion (Fig. 8). Indeed, the basicity of alumina is associated with the presence of surface O^- ions as counterpart of acid sites [51]. These basic sites adsorb carbon dioxide leading to an increase of CO_2 conversion and also methane conversion [52]. The effect of a stronger basicity, increasing CO_2 and CH_4 conversions was suggested by Wang et al. [53] investigating a series of Ce-promoted nickel catalysts ($NiCe_xC$). Moreover, Wen et al. [54] proposed that strong CO_2 adsorption on γ-Al_2O_3 plays an important role in CO_2 decomposition under corona discharges, favoring CO production. Using diffuse scattering IR spectroscopy Gadzhieva [55] showed that CH_4 adsorption sites were formed by molecular and dissociative mechanisms under the action of the electric-discharge plasma at the surface of γ-Al_2O_3.

So according to the results presented here and based on works of Chawdhury et al. [50] and D. Li [44] possible reaction pathways for CH_4 and CO_2 transformation into CO and H_2 is proposed in Fig. 9. The reaction takes place in gas phase under plasma discharge by electron-induced dissociation of reactants. Surface reactions are also involved, adsorption of methane can be followed by the cleavage of a C-H bond to produce surface CHx species. It is also possible to propose the adsorption of CHx formed in gas phase under plasma. CO_2 can also be activated directly in the gas phase or after adsorption leading to CO formation and a radical O able to react with CHx to produce CO.

3.4 Characterization of alumina materials before and after reaction under plasma

The BET specific surface area, BJH desorption cumulative pores volume and average pore width for the catalysts after reaction under plasma are gathered in Table 1. We observe a slight decrease of the surface area after plasma, except for Al_2O_3 400, while pore volumes remain constant. The pore size increases for γ–Al_2O_3 and Al_2O_3 800 and remains stable for the two other solids. TGA-TDA analysis reported in Fig. 10 exhibits mainly two weight loss in the temperature ranges 100-300 °C and 300-600 °C, corresponding respectively to hydroxyl and carbon elimination. TGA coupled with mass spectrometry analysis (Fig. 11) confirms that H_2O is eliminated at low temperature while carbon oxidation proceeds at the highest temperature (analysis of CO_2). The values of weight loss are also reported in Table 4 for the alumina materials before and after plasma. It appears that the amount of –OH groups differs significantly from one material to another one. As expected a higher calcination temperature (from 400 to 800 °C) leads to dehydroxylation. The lowest amount of hydroxyl is obtained with the commercial alumina due to its lowest surface area. After plasma, the amount of OH has significantly decreased for the commercial gamma alumina, from 3.3 % before plasma to 1.1 % after plasma. It indicates that dehydroxylation occurred under plasma, which could be related to the selectivity into oxygenates (Table 3) with the commercial alumina. The weight loss in the temperature range 300-600 °C is low after reaction indicating that carbon deposition is limited under the experimental conditions used in this study for the four alumina samples. Indeed the excess of CO_2 used in this study avoid carbon deposition by methane cracking.

3. Conclusion

The dry reforming of methane reaction was performed by coupling plasma with different types of alumina materials, while the granulometry was fixed in the range: 355-650 µm. Physical

characterization of the discharge through the Lissajous Q-V figures exhibited significant differences for the four alumina oxides. The lowest effective capacitance being obtained for the commercial alumina. As expected, excess of CO_2 (CO_2/CH_4 = 2) leads to a low carbon deposition, as evidenced by TGA analysis after reaction. We showed that besides γ-Al_2O_3 materials, the highest conversions were obtained with the commercial alumina, possessing the lowest surface area: 72 m^2 g^{-1}. Methane conversion reaches 31.3 % against 23.4, 22.6 and 26.8 % for alumina exhibiting surface area of 313, 301 and 261 m^2 g^{-1} respectively. These results suggest that the active sites generated into the mesoporosity of alumina synthesized in the laboratory are not accessible to reactants under the plasma discharge. A correlation between the number of acid and basic sites is clearly visible. The results obtained in the present study confirmed experimentally that the coupling of plasma with catalyst depends strongly on the nature of surface active species (presence of OH) but in a lower extend to the amount of active sites as soon as there are located in small pores of oxides.

Acknowledgements

The authors grateful acknowledge the ANR for the financial support of the PRC program VALCO2PLAS and the financial support from the European Union (ERDF) and "Région Nouvelle Aquitaine".

References

[1] C. Barakat, P. Gravejat, O. Guaitella, F. Thevenet, A. Rousseau, Oxidation of isopropanol and acetone adsorbed on TiO_2 under plasma generated ozone flow: gas phase and adsorbed species monitoring, Appl. Catal. B (2014) 147, 302–13

[2] J. Hong, S. Prawer, A.B. Murphy, Plasma catalysis as an alternative route for ammonia production: status, mechanisms, and prospects for progress ACS Sustain. Chem. Eng. (2018) 6, 15–31

[3] H. Puliyalil, D.L. Jurkovic, V.D. Dasireddy, B. Likozar, B. A review of plasma-assisted catalytic conversion of gaseous carbon dioxide and methane into value-added platform chemicals and fuels. RSC Adv. 8 (2018) 27481-27508.

[4] R. Dębek, F. Azzolina-Jury, A. Travert, F. Maugé, A review on plasma-catalytic methanation of carbon dioxide – Looking for an efficient catalyst, Renewable and Sustainable Energy Reviews 116 (2019) 109427.

[5] M. Mikhail, P. Da Costa, J. Amouroux, S. Cavadias, M. Tatoulian, S. Ognier, M. E. Gálvez, Electrocatalytic behaviour of CeZrOx-supported Ni catalysts in plasma assisted CO_2 methanation, Catal. Sci. Technol. (2020) 10, 4532

[6] L. Jia, Al Farouha, L. Pinard, , S. Hedan, J.-D Comparot, A. Dufour, K. Ben Tayeb, H. Vezin and C. Batiot-Dupeyrat, New routes for complete regeneration of coked zeolite, Appl. Catal. B: Env, 219 (2017) 82-91

[7] A. Bogaerts, X. Tu, J.C. Whitehead, G. Centi, L. Lefferts, O. Guaitella, F. Azzolina-Jury, H.H. Kim, A.B. Murphy, W.F. Schneider, T. Nozaki, J.C. Hicks, A. Rousseau,F. Thevenet, A. Khacef, M. Carreon, The 2020 plasma catalysis roadmap, J. Phys. D Appl. Phys. 53 (2020), 443001.

[8] E.C. Neyts, A. Bogaerts, Understanding plasma catalysis through modelling and simulation - A review. J. Phys. D Appl. Phys. 47 (2014) 224010.

[9] A.J. Zhang, A.M. Zhu, J. Guo, Y. Xu, C. Shi, Conversion of greenhouse gases into syngas via combined effects of discharge activation and catalysis, Chem Eng J, 156 (2010) 601–606.

[10] M. Kraus, W. Egli, K. Haffner, B. Eliasson, U. Kogelschatz, A. Wokaun, Investigation of mechanistic aspects of the catalytic CO_2 reforming of methane in a dielectric-barrier discharge

using optical emission spectroscopy and kinetic modeling, Phys Chem Chem Phys 4 (2002) 668–675.

[11] J. Sentek, K. Krawczyk, M. Młotek, M. Kalczewska, T. Kroker, T. Kolb, A. Schenk, H. Gericke, K. Schmidt-Szałowski, Plasma-catalytic methane conversion with carbon dioxide in dielectric barrier discharges, Appl. Catal. B 94 (2010) 19–26.

[12] A. H. Khoja, M. Tahir, N. A. S. Amin . Recent developments in non-thermal catalytic DBD plasma reactor for dryreforming of methane, En. Conv. Management, 183 (2019) 529-560.

[13] D. Ray, D. Nepak, S. Janampelli, P. Goshal, C. Subrahmanyam, Dry reforming of methane in DBD plasma over Ni-based catalysts: influence of process conditions and support on performance and durability, Energy Technol. 7 (2019), 1801008.

[14] D. Mei, B. Ashford, Y.L. He, X. Tu, Plasma-catalytic reforming of biogas over supported Ni catalysts in a dielectric barrier discharge reactor: effect of catalyst supports, Plasma Process. Polym. 14 (2017), 1600076.

[15] D.G. Cheng, X. Zhu, Y. Ben, F. He, L. Cui, C.J. Liu, Carbon dioxide reforming of methane over Ni/Al_2O_3 treated with glow discharge plasma, Catal. Today, 115 (2006) 205-210

[16] X. Tu, J.C. Whitehead, Plasma-catalytic dry reforming of methane in an atmospheric dielectric barrier discharge: Understanding the synergistic effect at low temperature. Appl. Catal. B Environ. 125 (2012) 439-448.

[17] A. Aziznia, H.R. Bozorgzadeh, N. Seyed-Matin, M. Baghalha, A.Mohamadelizadeh, Comparison of dry reforming of methane in low temperature hybrid plasma-catalytic corona with thermal catalytic reactor over $Ni/\gamma\text{-}Al_2O_3$. J. Nat. Gas Chem. 21 (2010) 333-347.

[18] X. Tu, H.J. Gallon, M.V. Twigg, P.A. Gorry, J.C. Whitehead, Dry reforming of methane over a Ni/Al_2O_3 catalyst in a coaxial dielectric barrier discharge reactor. J. Phys. D Appl. Phys. 44 (2011) 274007-274017.

[19] S. Jo, T.Kim, D.H. Lee, W.S. Kang, Y.H. Song, Y.H. Effect of the electric conductivity of a catalyst on methane activation in a dielectric barrier discharge reactor. Plasma Chem. Plasma Process. 34 (2014) 175-186.

[20] J. Kim, M.S. Abbott, D.B.Go, J.C. Hicks, Enhancing C–H Bond Activation of Methane via Temperature-Controlled, Catalyst–Plasma Interactions. ACS Energy Lett. 1 (2016) 94-99.

[21] W.C. Chung, M.B. Chang, Review of catalysis and plasma performance on dry reforming of CH_4 and possible synergistic effects, Renew. and Sustain. En. Rev., 62 (2016) 13-31.

[22] T. Jiang, Y. Li, C.J. Liu, G.H. Xu, B. Eliasson, B. Xue, Plasma methane conversion using dielectric-barrier discharges with zeolite A. Catal. Today 72 (2002) 229-235.

[23] R. Vakili, R. Gholami, C. E. Stere, S. Chansai, H. Chen, S. M. Holmes, Y. Jiao, C. Hardacre, X. Fan, Plasma-assisted catalytic dry reforming of methane (DRM) over metal-organic frameworks (MOFs)-based catalysts, Appl. Catal. B: Env. 260 (2020) 118195

[24] D. Yap, J.M. Tatibouët, C. Batiot-Dupeyrat, Catalyst assisted by non-thermal plasma in dry reforming of methane at low temperature, Catal. Today, 299 (2018) 263-271.

[25] X. Zhang, B. Dai, A.Zhu, W. Gong, C. Liu, C, The simultaneous activation of methane and carbon dioxide to C2 hydrocarbons under pulse corona plasma over La_2O_3/γ-Al_2O_3 catalyst Catal. Today 72 (2002) 223-227.

[26] I. Michielsen , Y. Uytdenhouwen, A. Bogaerts, V. Meynen, Altering conversion and product selectivity of dry reforming of methane in a dielectric barrier discharge by changing the dielectric Packing Material, Catalysts (2019) 51

[27] N. Bouchoul, E. Fourré, A. Duarte, N. Tanchoux, C. Louste, C. Batiot-Dupeyrat, Plasma-metal oxides coupling for CH_4-CO_2 transformation into syngas and/or hydrocarbons, oxygenates, Catal. Today, in press 2021, doi10.1016/j.cattod.2020.06.058

[28] N. Bouchoul, E. Fourré, J.M. Tatibouët, C. Batiot-Dupeyrat, Plasma-Catalytic dry reforming of CH_4 over calcium oxide: Catalyst structural and textural modifications, Plasma Chem. Plasma Process. 39 (2019) 713-727

[29] Kasinathan P, Park S, Choi WC, Hwang YK, Chang JS, Park YK, Plasma-Enhanced Methane Direct Conversion over Particle-Size Adjusted MOx/Al_2O_3 (M = Ti and Mg) Catalysts Plasma Chem Plasma Process, 34 (2004) 1317–1330

[30] Zhou, A., Chen, D., Ma, C., Yu, F., Dai, B., DBD Plasma-ZrO_2 catalytic decomposition of CO_2 at Low Temperatures, Catalysts, 8 (2018) 256

[31] Z-Y. Yuan, T-Z. Ren, A. Vantomme, B-L. Su, Facile and Generalized Preparation of Hierarchically Mesoporous−Macroporous Binary Metal Oxide Materials, Chem. Mater. 16 (2004) 5096-5106.

[32] S. Célerier, S. Morisset, I. Batonneau-Gener, T. Belin, K. Younes, C. Batiot-Dupeyrat, Glycerol dehydration to hydroxyacetone in gas phase over copper supported on magnesium oxide (hydroxide) fluoride catalysts, Applied Catalysis A: General 557 (2018) 135–144.

[33] M. Thommes, K. Kaneko, A. V. Neimark, J. P. Olivier, F. Rodriguez-Reinoso, J. Rouquerol, Physisorption of Gases, with Special Reference to the Evaluation of Surface Area and Pore Size Distribution, Pure and Applied Chem. 87, 9-10 (2015) 1051-1069.

[34] S. Jo, D.H. Lee, W.S. Kang, Y.H. Song, Methane activation using noble gases in a dielectric barrier discharge reactor, Physics of plasmas, 20 (2013) 123507-8.

[35] J. Robertson, High dielectric constant oxides, Eur. Phys. J. Appl. Phys. 28 (2004) 265-291.

[36] W. Wang, H.H. Kim, K. Van Laer, A. Bogaerts, Streamer propagation in a packed bed plasma reactor for plasma catalysis applications, Chem. Eng. J 334 (2018) 2467-2479.

[37] M. Taheraslani, H. Gardeniers, Coupling of CH_4 to C2 Hydrocarbons in a Packed Bed DBD Plasma Reactor: The Effect of Dielectric Constant and Porosity of the Packing, Energies 13 (2020) 468-487.

[38] H Lin, W. Xu, H. Zhang, C. Chen, Y. Zhou, Z. Yi, Origin of high dielectric performance in fine grain-sized $CaCu_3Ti_4O_{12}$ materials, J. Eur. Ceramic Society 40 (2020) 1957–1966.

[39] Y.R. Zhang, K.Van Laer, E. C. Neyts, A. Bogaerts, Can plasma be formed in catalyst pores? A modeling investigation, Appl. Catal. B: Environ., 185 (2016) 56-67.

[40] Q.Z. Zhang, A. Bogaerts, Propagation of a plasma streamer in catalyst pores, Plasma Sources Sci. technol. 27 (2018) 35009-35019.

[41] F. Holzer, U. Roland, F. D. Kopinke, Combination of non-thermal plasma and heterogeneous catalysis for oxidation of volatile organic compounds, Part 1. Accessibility of the intra-particle volume, Appl. Catal. B: Environ. 38 (2002) 163-181

[42] U. Roland, F. Holzer, A. Pöppl, F.D. Kopinke, Combination of non-thermal plasma and heterogeneous catalysis for oxidation of volatile organic compounds, Part 3. Electron paramagnetic resonance (EPR) studies of plasma-treated porous alumina, Appl. Catal. B: Environ. 58 (2005) 227-234

[43] C. De Bie, J. Van Dijk, A. Bogaerts, The dominant pathways for the conversion of methane into oxygenates and syngas in an atmospheric pressure dielectric barrier discharge, J. Phys. Chem. C 119 (2015) 22331-22350.

[44] D. Li, V. Rohani, F. Fabry, A. P. Ramaswamya, M. Sennour, L. Fulcheri, Direct conversion of CO_2 and CH_4 into liquid chemicals by plasma-catalysis, Appl. Catal. B: Environ. 261 (2020) 118228

[45] H.J. Gallon, X. Tu, J.C. Whitehead, Effects of reactor packing materials on H_2 production by CO_2 reforming of CH_4 in a dielectric barrier discharge, Plasma Process. and polymer, 9 (2012) 90-97

[46] H.K. Song, J.W. Choi, S.H. Yue, H. Lee, B.K. Na, Synthesis gas production via dielectric barrier discharge over Ni/ γ-Al_2O_3 catalyst, Catal. Today, 89 (2004) 27-33

[47] H. Long, S. Shang, X. Tao, Y. Yin, X. Dai, CO_2 reforming of CH_4 by combination of cold plasma jet and Ni/ γ-Al_2O_3 catalyst, Int. J. of Hydr. En. 33 (2008) 5510-5515

[48] G. Busca, Chapter Three - Structural, Surface, and Catalytic Properties of Aluminas. Advances in Catalysis 57 (2014) 319- 404.

[49] X. Liu, X., R.E.Truitt, DRFT-IR Studies of the Surface of γ-Alumina. J. Am. Chem. Soc., 119, 41 (1997) 9856-9860.

[50] P. Chawdhury, Y. Wang, D. Ray, S. Mathieu, N. Wang , J. Harding, F. Bin, X. Tu, Ch. Subrahmanyam, promising plasma-catalytic approach towards single-step methane conversion to oxygenates at room temperature, Appl. Catal. B: Environ., 284 (2021) 119735

[51] J. Medema, Isomerization of butene over alumina, Journal of Catalysis, 37, 1 (1975) 1, 91-100.

[52] S. K. Kundu, E.M. Kennedy, V.V. Gaikwad, T.S. Molloy, B.Z. Dlugogorski, Experimental investigation of alumina and quartz as dielectrics for a cylindrical double dielectric barrier discharge reactor in argon diluted methane, Plasma Chem. Eng. J. 180 (2012) 178-189.

[53] H. Wang, B. Zhao, L. Qin, Y. Wang, F. Yu, J. Han, Non-thermal plasma-enhanced dry reforming of methane and CO_2 over Ce promoted Ni/C catalysts, Molecular Catalysis 485 (2020) 110821

[54] Wen, H., Jiang, X., Decomposition of CO_2 using pulsed corona discharges combined with catalyst, Plasma Chem. Plasma Process., 21 (2001) 665-677

[55] Gagdzhieva, N.N., Methane adsorption and plasma-assisted catalytic conversion on the surface of γ- alumina, Plasma Chemistry, 37 (2003) 43-49

Table 1. Characterization of alumina materials, S_{BET}, pore volume and pore size before and after plasma

Alumina	S BET[a] ($m^2 .g^{-1}$)		Pore volume[b] ($cm^3.g^{-1}$)		Pore size[c] (Å)	
	Before plasma	After plasma	Before plasma	After plasma	Before plasma	After plasma
γ-Al_2O_3	72	55	0.2	0.2	142	165
Al_2O_3 400	313	334	0.6	0.7	61	61
Al_2O_3 600	301	275	0.7	0.7	72	71
Al_2O_3 800	261	165	0.3	0.6	42	104

a. Specific surface area calculated by the BET method.
b. Total pore volume determined at P/P_0=0.99.
c. Average pore width deduced from the BJH method using the desorption branch.

Table 2. Physical characterization of the materials dielectric constant and resulting capacitances of the reactor filled with the different alumina materials

Alumina	Dielectric constant		Capacitance	
	800 Hz	1 MHz	$C_{dielectric}$ (pF)	$C_{effective}$ (pF)
γ-Al_2O_3	3.07	2.94	9	22
Al_2O_3 400	4.11	3.30	13	32
Al_2O_3 600	3.79	3.23	16	39
Al_2O_3 800	3.97	2.90	10	25

Table 3. Influence of the nature of alumina on product selectivity and hydrogen yield (average value, reaction time: 30 minutes), grain size: 355-650 µm, P = 8 W, total flow: 40 mL min^{-1}, CO_2/CH_4 = 2, He: 75 %.

catalyst	H_2 yield (%)	Selectivity (%)			CB (%)
		CO	C_2H_6	Oxy.*	
γ-Al_2O_3	12.0	70	8.8	2.3	83
Al_2O_3 400	7.8	71	6.7	0.0	78
Al_2O_3 600	8.4	69	8.8	0.0	77
Al_2O_3 800	7.8	65	6.4	0.0	72

***** oxy. = oxygenates

Table 4. Mass loss from TGA analysis, before and after plasma (1 h, grain size: 355-650 µm, P = 8 W, total flow: 40 mL·min^{-1}, CO_2/CH_4 = 2, He: 75 %)

Oxide	Mass loss (%)			
	before plasma		after plasma	
	100-300°C	300-600°C	100-300°C	300-600°C
γ-Al_2O_3	3.3	1.7	1.1	3.2
Al_2O_3 400	5.1	2.6	5.8	4.7
Al_2O_3 600	6.0	2.5	3.2	3.0
Al_2O_3 800	3.7	1.7	3.6	4.1

Table 5. Performance of plasma + alumina processes

Plasma type	CH_4/CO_2	Flow ($mL.min^{-1}$)	P (W)	T (°C)	packing	shape	size	Conversion (%)		Selectivity (%)		comments	Ref.
								CH_4	CO_2	CO	HC		
DBD	1	33	19	240	α-Al_2O_3	beads	1-2 mm	36.5	21.9	19	43	P= 1.2 bar, 24% C_2H_6	11
DBD	1	50	100	room	α-Al_2O_3	sphere	2-2.24 mm	33	22.5	72.2	18.5		26
DBD	1	50	100	room	γ-Al_2O_3	sphere	2-2.24 mm	32	14	70.1	18.0		26
DBD	1	50	35	room	γ-Al_2O_3	pellets	500-850µm	22.5	7.5	32.5	17	CB=92%, 9% C_2H_6	43
DBD	1	30	130	room	γ-Al_2O_3	beads	1-2 mm	50.3	30	50	18		44
Plasma jet	0.7	16660	770	room	γ-Al_2O_3	n.i.	n.i.	45	30	86	n.i.		45

n.i.: not indicaded

Figure 1: Plasma reactor scheme

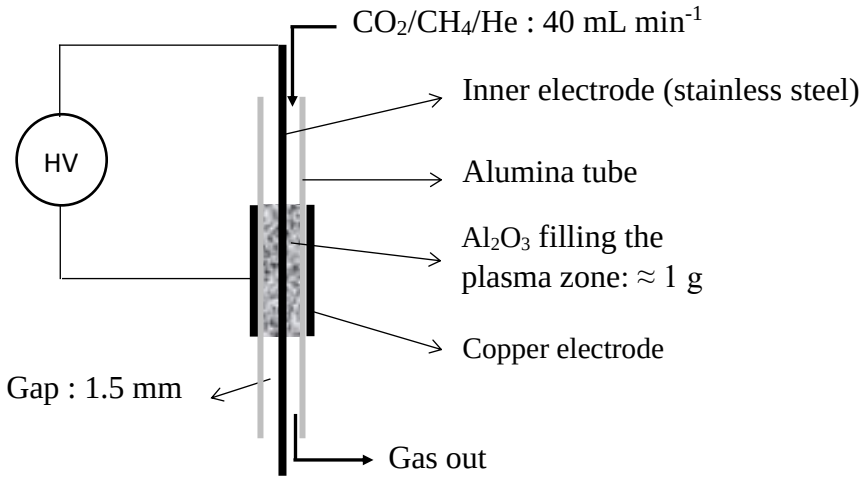

Figure 2: N_2 sorption isotherms and pore size distributions of the Al_2O_3 materials

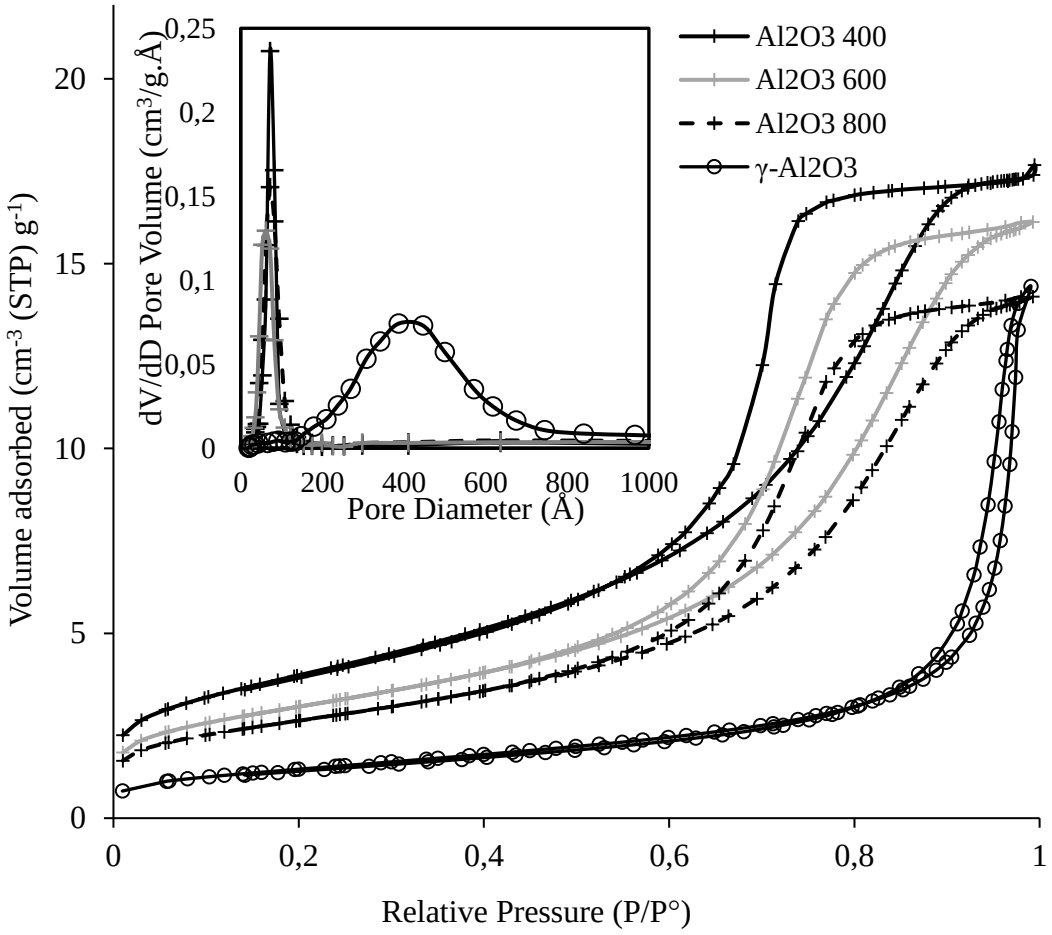

Figure 3: SEM images of the Al_2O_3 materials calcined at different temperatures, a), b) 400 °C, c), d) 600 °C and e), f) 800 °C

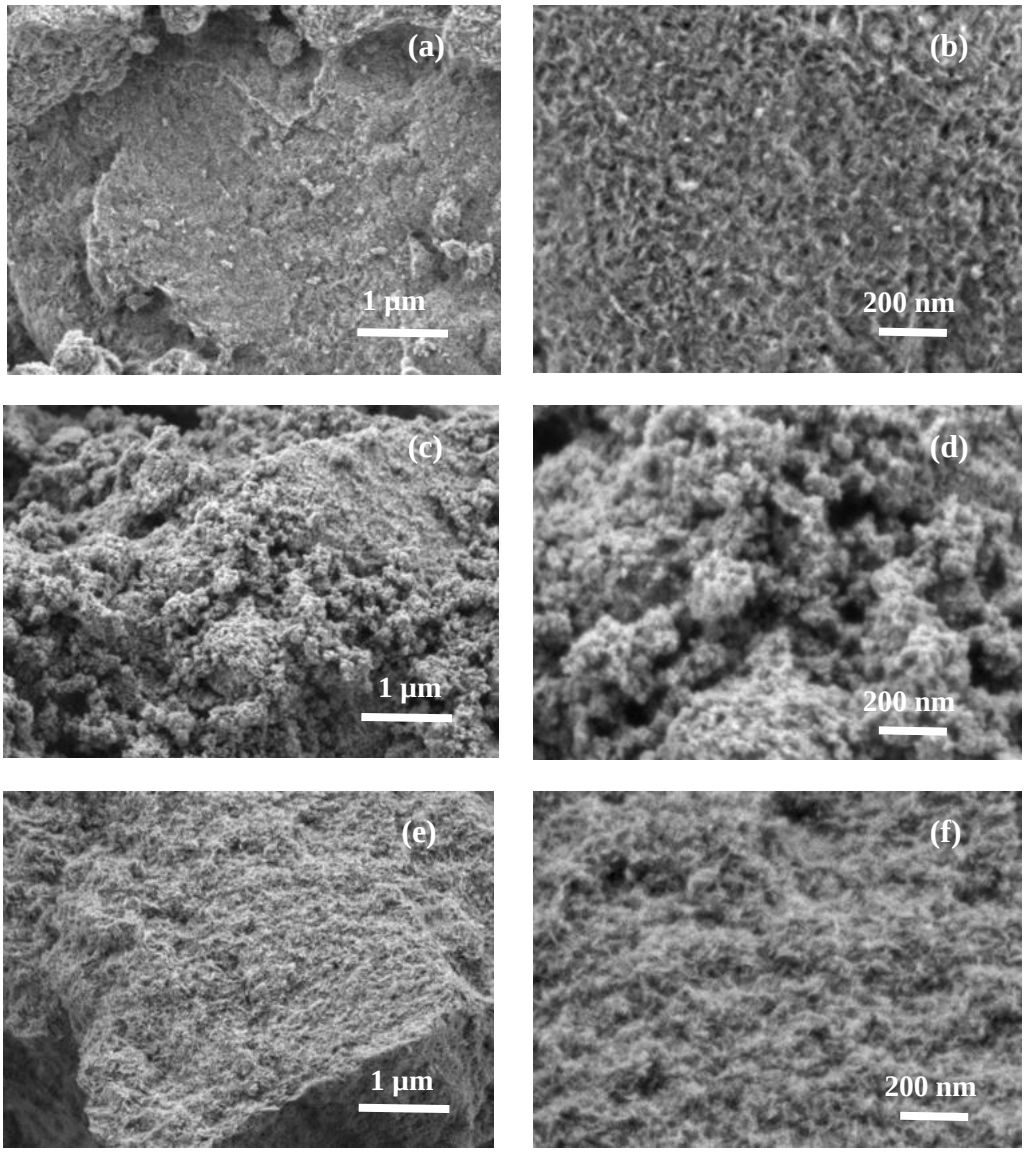

Figure 4: XRD patterns of commercial γ- Al_2O_3, Al_2O_3 400, Al_2O_3 600 and Al_2O_3 800.

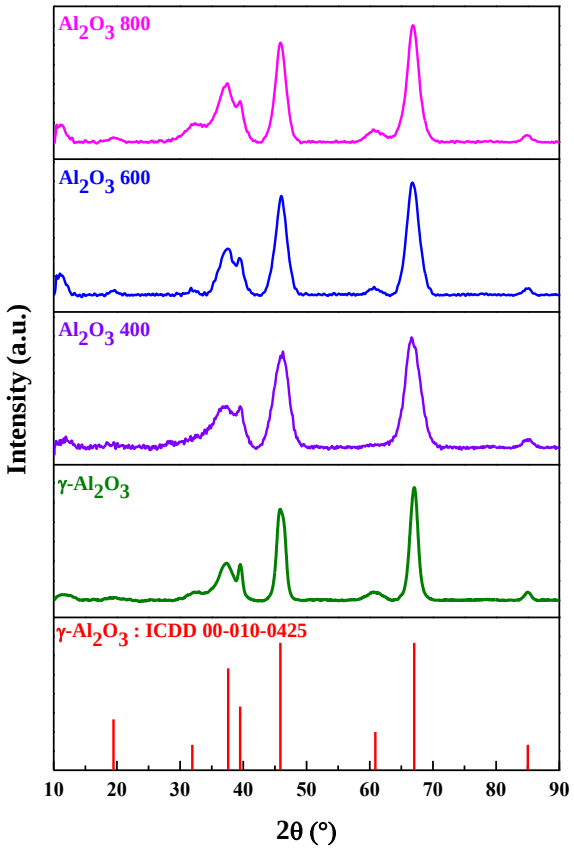

Figure 5: Lissajous figures of the CH_4/CO_2/He DBD with alumina materials and typical Lissajous figure of DBD

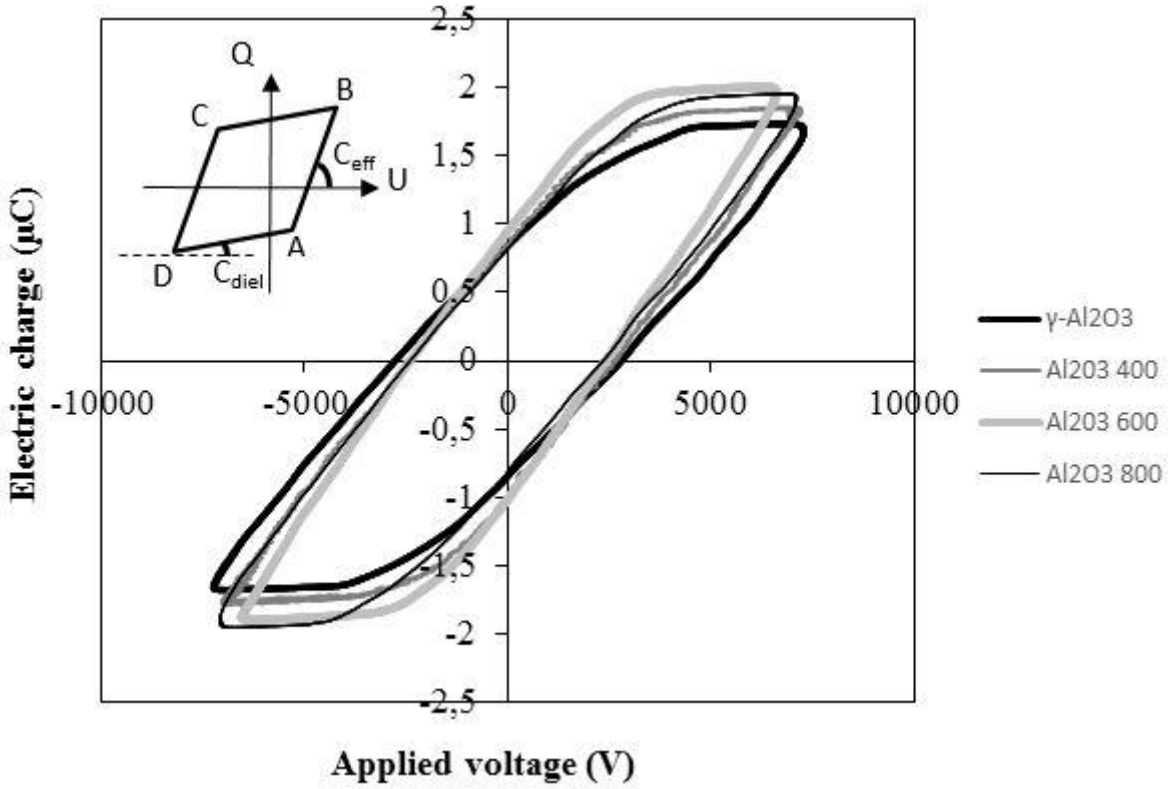

Figure 6: CH_4 and CO_2 conversion versus surface area for alumina, grain size: 355-650 µm, P = 8 W, total flow: 40 mL min^{-1}, CO_2/CH_4 = 2, He: 75 %

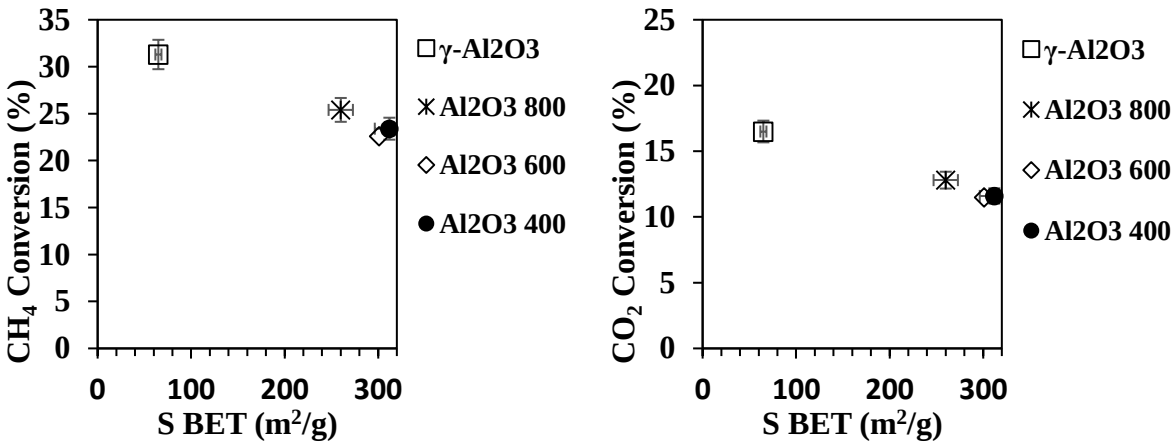

Figure 7: CH_4 and CO_2 conversion versus number of acid sites for alumina, grain size: 355-650 µm, P = 8 W, total flow: 40 mL·min^{-1}, CO_2/CH_4 = 2, He: 75 %

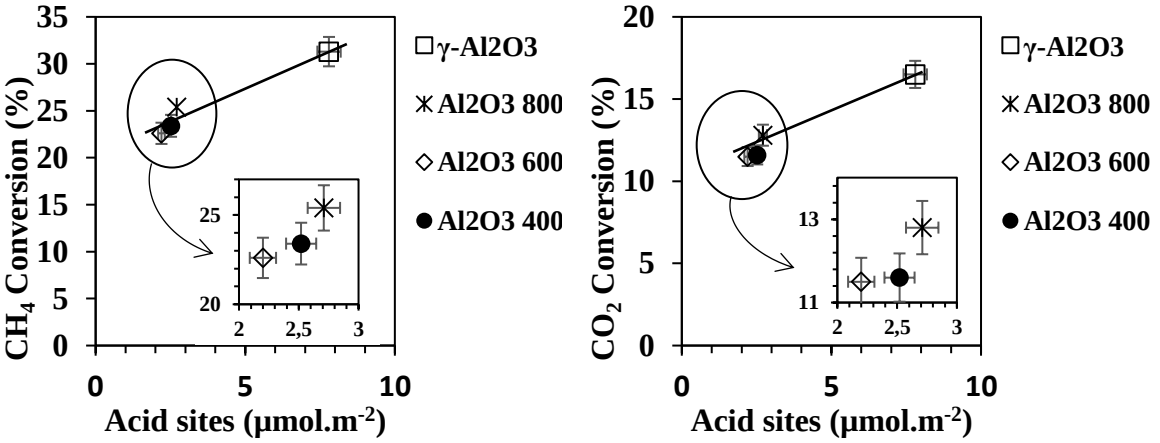

Figure 8: CH_4 and CO_2 conversion versus number of basic sites for alumina, grain size: 355-650 µm, P = 8 W, total flow: 40 mL min^{-1}, CO_2/CH_4 = 2, He: 75 %

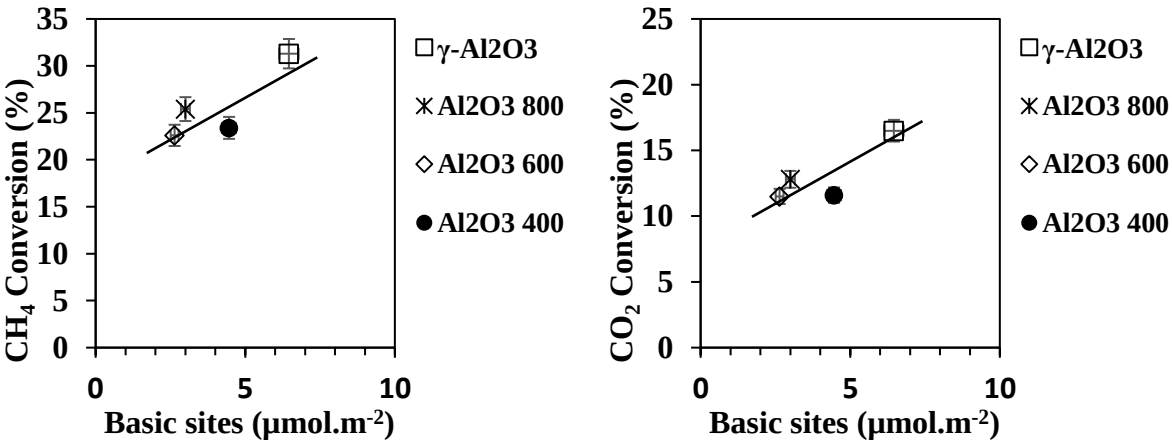

Figure 9: Suggested reaction pathways for the transformation of methane and carbon dioxide in the plasma-catalytic system in the presence of γ-Al_2O_3

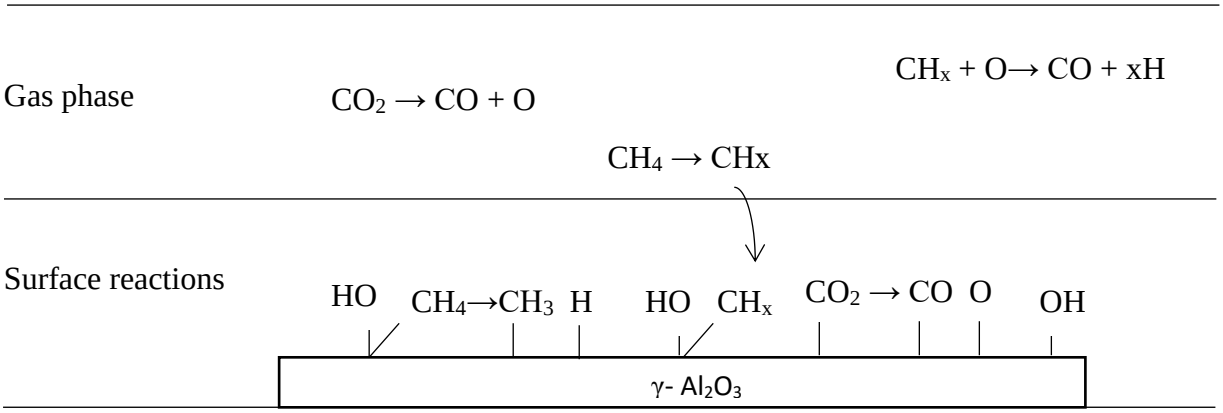

Figure 10: TGA-TDA analysis before and after reaction under plasma (60 minutes), grain size: 355-650 µm, P = 8 W, total flow: 40 mL min^{-1}, CO_2/CH_4 = 2, He: 75 %,

before plasma, after plasma

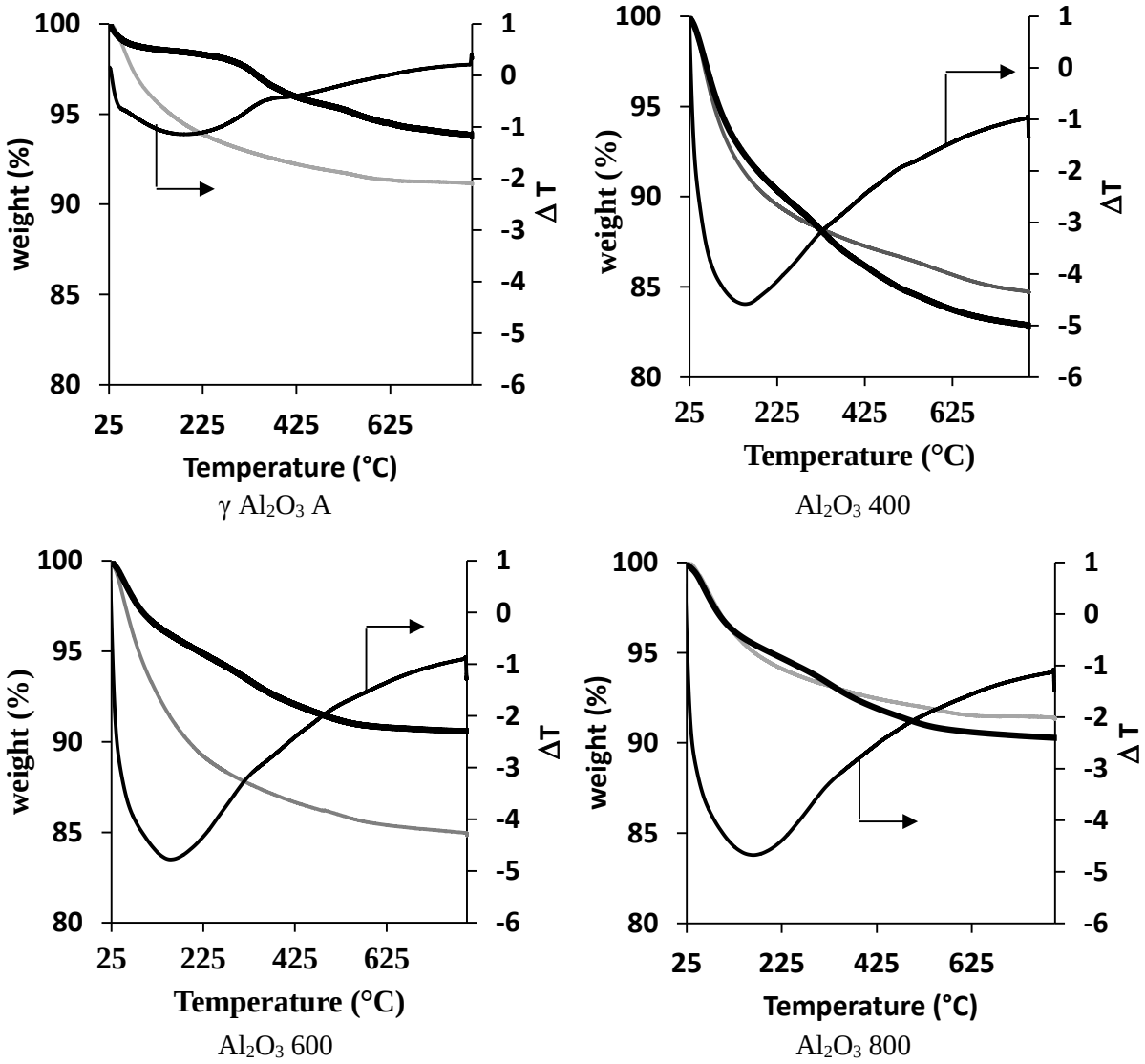

γ Al_2O_3 A

Al_2O_3 400

Al_2O_3 600

Al_2O_3 800

Figure 11: TGA-MS analysis after reaction under plasma (60 minutes), Al_2O_3 800, grain size: 355-650 µm, P = 8 W, total flow: 40 mL·min^{-1}, CO_2/CH_4 = 2, He: 75 %